Polewards Microtubule Flux in the Mitotic Spindle: Evidence from Photoactivation of Fluorescence

T. J. Mitchison

Department of Pharmacology, University of California, San Francisco, California, 94143-0405

Abstract. I have synthesized a novel derivative of carboxyfluorescein that is nonfluorescent, but can be converted to a fluorescent form by exposure to 365-nm light. This photoactivable, fluorescent probe was covalently attached to tubulin and microinjected into mitotic tissue culture cells, where it incorporated into functional spindles. To generate a fluorescent bar across the mitotic spindle, metaphase cells were irradiated with a slit microbeam. This bar decreased in intensity over the first minute, presumably due to turnover of nonkinetochore microtubules. The remaining fluorescent zones, now presumably restricted to kinetochore microtubules, moved polewards at 0.3–0.7 μm/min. This result provides strong evidence for polewards flux in kinetochore microtubules. In conjunction with earlier biotin-tubulin incorporation experiments (Mitchison, T. J., L. Evans, E. Schulze, and M. Kirschner. 1986. *Cell.* 45:515–527), I conclude that microtubules polymerize at kinetochores and depolymerize near the poles throughout metaphase. The significance of this observation for spindle structure and function is discussed. Local photoactivation of fluorescence should be a generally useful method for following molecular dynamics inside living cells.

THE mitotic spindle is a spatially organized array of microtubules that effects the accurate segregation of sister chromatids during cell division. The metaphase spindle can maintain the same average structure for long periods, but it is known to be highly dynamic. It responds quickly to conditions perturbing tubulin polymerization (Inoue and Sato, 1967), exchanges rapidly with soluble tubulin subunits (Salmon et al., 1984; Saxton et al., 1984), and exhibits continuous oscillations of chromosomes parallel to the spindle axis (Bajer, 1982). To understand the structure and assembly of the mitotic spindle, we need to understand its dynamic behavior. For microtubule arrays (and probably most cytoplasmic assemblies) structure and dynamics are intimately related (Kirschner and Mitchison, 1986). The dynamic behavior of kinetochore microtubules is particularly important, because it is directly related to the mechanisms by which chromosomes are aligned at the metaphase plate and subsequently segregated (Nicklas, 1971). These dynamics are likely to reflect the inherent polymerization dynamics of the microtubule lattice (Kirschner and Mitchison, 1986), modulated by microtubule binding proteins and force-producing ATPases localized in the kinetochore and other parts of the spindle (Mitchison, 1988*a*).

Microinjection of biotin-labeled tubulin subunits has shown that kinetochore microtubules polymerize at the kinetochore throughout metaphase (Mitchison et al., 1986; Mitchison, 1988*b*). This experiment, together with in vitro studies (Mitchison and Kirschner, 1985) showed that the microtubule-kinetochore interface is dynamic, allowing subunit addition to microtubule ends without loss of attachment. Labeled microtubule segments at the kinetochore progressively increased in the length with time. The simplest explanation of this observation was that kinetochore microtubules move polewards during metaphase, polymerizing at kinetochores and depolymerizing at the poles, i.e., that they exhibit polewards flux. However labeled microtubule segments at the kinetochore could have arisen from two other mechanisms: (*a*) detachment of individual microtubules, depolymerization, repolymerization, and reattachment; and (*b*) polymerization and depolymerization at microtubule plus ends attached to kinetochores during chromosome movement. This would result in label incorporation into a zone around the spindle equator swept out by oscillating chromosomes. In fact, both mechanisms probably do occur in vivo (see Discussion). Because these mechanisms could have accounted for the labeled subunit incorporation into microtubules at kinetochores, proving the existence of flux requires demonstrating that the polymer lattice of kinetochore microtubules actually moves polewards.

To assay movement of microtubules in the spindle directly, it is necessary to follow marks that remain at a fixed position on the polymer lattice. Such marks would ideally be restricted to kinetochore microtubules, and could be endogenous or experimentally produced. Naturally existing anisotropic features of the spindle such as small particles (Bajer, 1967) and variations in birefringence (Schaap and Forer, 1984) have been followed, but their relation to the polymer lattice of kinetochore microtubules was undefined. Local ablation of kinetochore microtubules with an ultraviolet microbeam generated marks on kinetochore fibers that progressed

polewards (Forer, 1965). However, this technique may have measured the polymerization dynamics of the new microtubule ends rather than endogenous dynamics. More recently, fluorochromes have been covalently attached to tubulin subunits and microinjected into mitotic cells, leading to uniform spindle labeling. Local photobleaching using high-intensity laser pulses was then used to generate marked zones on microtubules. Most of the fluorescence in the bleached zones recovered rapidly, demonstrating that the majority of spindle microtubules turn over rapidly (Salmon et al., 1984; Saxton et al., 1984). The rapid turnover of nonkinetochore microtubules tends to obscure the behavior of the less dynamic kinetochore microtubules. These and subsequent photobleaching studies observed no vectorial transport of bleached zones, and thus concluded that marked zones on kinetochore microtubules remain stationary with respect to the spindle pole both in metaphase (Wadsworth and Salmon, 1986; Gorbsky and Borisy, 1989) and anaphase (Gorbsky et al., 1988), implying the absence of polewards flux. However, one photobleaching study has provided limited evidence of polewards flux in metaphase spindles of sand dollar embryos (Hamaguchi et al., 1987).

To try and resolve the contradiction between the results of biotin-tubulin incorporation and photobleaching experiments I have developed a new method for marking microtubules inside cells: photoactivation of fluorescence. The principle is to generate fluorescent marks on microtubules on a dark background, instead of the reverse as in photobleaching. Kinetochore microtubules exchange subunits more slowly than other spindle microtubules (Salmon and Begg, 1980; Mitchison et al., 1986). A mark made on all spindle tubulin by photoactivation of fluorescence should rapidly convert to a mark on kinetochore microtubules alone, as soluble subunits diffuse and nonkinetochore microtubules turn over. Thus, the method is ideal for following kinetochore microtubules, provided a probe can be designed that is compatible with normal tubulin function. In photobleaching experiments, kinetochore microtubules can only be followed with some difficulty as zones of reduced fluorescence on a bright background (Wadsworth and Salmon, 1986). In general, photoactivation of fluorescence has a theoretical advantage in signal-to-noise over fluorescence photobleaching, which may be most telling when tracking the least dynamic component of a complex system (Krafft et al., 1986). Photoactivation has a second theoretical advantage in that appropriate design of the photochemical reaction should allow marking of microtubules using light of appropriate wavelength to produce a defined chemical change without side reactions. Although careful photobleaching studies now give reliable protein diffusion rates (reviewed in Jacobsen et al., 1987), the method can potentially lead to artifacts from local heating, photochemical cross-linking, and oxygen radical–induced damage (Leslie et al., 1984; Vigers and McIntosh, 1988).

To generate fluorescent zones on spindle microtubules, I have synthesized a novel nonfluorescent derivative of carboxyfluorescein that is readily photolyzed to generate a highly fluorescent molecule. I report here the results from photoactivation experiments during metaphase that have important consequences for our understanding of spindle dynamics and structure.

Materials and Methods

Synthesis of Bis-caged-Fluorescein Probe

All steps were performed under orange photographic safe light for both the reagent synthesis and the subsequent tubulin labeling. All chemicals were from Aldrich Chemical Co. (Milwaukee, WI) except where indicated and were used without further purification. TLC was performed on silica-gel plates (type PE SIL G/UV; Whatman Instruments, Maidstone, UK). Solvent system A was composed of 66% benzene and 33% acetone. System B was composed of 83% benzene and 17% acetone. System C was made up of 50% benzene, 48% acetone, 2% acetic acid. Numbered compounds refer to Fig. 1 *B*. All compounds were a mixture of 5- and 6-isomers of the R1 groups.

Compound 2. 13.2 g (35 mmol) (5 or 6)-carboxy fluorescein (Eastman Kodak Co., Rochester, NY), and 4.1 g (35.6 mmol) *N*-hydroxysuccinimide were dissolved in 100 ml dimethylformamide (anhydrous sure-seal grade). 7.2 g (35 mmol) of dicyclohexyl carbodiimide was added and the mixture was stirred for 10 h at room temperature. Dicyclohexylurea was removed by vacuum filtration. 5.4 g (35 mmol) of β-alanine-ethylester-hydrochloride (Sigma Chemical Co., St. Louis, MO) was added, followed by 10 ml (70 mmol) of triethylamine. After 2 h at room temperature, the mixture was filtered and the solvent mostly removed by vacuum evaporation. The residue was partitioned between 300 ml of 1 M $NaHSO_4$ and 300 ml diethylether. The aqueous phase was reextracted three times with ether and the pooled ether phase was dried over $MgSO_4$. Filtration and vacuum evaporation followed by several days at high vacuum yielded 16.4 g of crude compound 2 (relative fluorescence [rf][1] 0.63 in system A). Compound 2 was contaminated by unreacted carboxy-fluorescein and other minor fluorescent contaminants. It was used "as is" for the next step, or sometimes purified in aliquots by column chromatography on silica gel (cat. no. 28,859-4; Aldrich Chemical Co.) in system A.

Compound 3. 2.3 g (5 mmol) compound 2 and 2.2 g (10 mmol) of *o*-nitrobenzyl-bromide were dissolved in 10 ml of tetrahydrofuran (anhydrous sure-seal grade); 60 ml of benzene dried over molecular sieves were added followed by 2.8 g (12 mmol) silver(I)oxide. The mixture was refluxed with a drying tube for 12 h, to give a mixture of products that could be resolved by TLC in system B. Compound 3, the major product, was easily identified as a double spot (rf = 0.4). It initially showed little color in visible light, no fluorescence when illuminated at 360 nm, and dark absorption when illuminated at 260 nm. After 30 s of illumination at 260 nm, the dark absorption changed to yellow fluorescence, illumination at 360 nm induced bright yellow-orange fluorescence, and the spots appeared yellow in visible light. This property of photoactivating on the TLC plate was diagnostic of compounds 3–5. The monocaged ether adduct was identified as a yellow fluorescent spot (rf = 0.18), which was prominent early in the reaction and then disappeared. The reaction mixture was filtered and vacuum was evaporated to dryness. It was then subject to flash chromatography as above in solvent system B. The fractions were examined by TLC in system B, and fractions were pooled that contained the product but not other fluorescent species. An unidentified fluorescent contaminant chromatographing slightly ahead of the product was difficult to separate, lowering the yield. The 5- and 6-isomers of the product separated slightly on the column, and the product was usually enriched in the slower migrating one (not identified). Pure fractions were pooled and vacuum evaporated to dryness to yield 0.9 g of compound 3 (25% yield).

Compound 4. 0.9 g (1.2 mmol) compound 3 was dissolved in 10 ml benzene. 20 ml methanol was added, followed by 1 ml 5 M NaOH. The mixture was incubated at room temperature for 1–2 h, until all the ester was hydrolyzed. The reaction was followed by TLC of small aliquots which were acidified and examined in system B. Compound 4 had rf = 0. When hydrolysis was complete, the mixture was partitioned between 1 M $NaHSO_4$ and chloroform. The organic phase was dried over $MgSO_4$ and vacuum evaporated to dryness.

Compound 5. The residue from the last step was weighed (0.7 g, 1 mmol) and taken up in 5.5 ml of DMSO (anhydrous sure-seal grade) containing 0.24 g (1.1 mmol) *N*-hydroxy-sulfo-succinimide, sodium salt (Pierce Chemical Co., Rockford, IL). 0.21 g (1 mmol) of dicyclohexylcarbodiimide was added, and the mixture was incubated overnight at room temperature. The reaction was monitored by TLC in solvent A, in which compound 4 smeared up off the origin, whereas compound 5 (C2CF-SNHS) stayed right at the

1. *Abbreviations used in this paper*: BRB80, 80 mM K Pipes, 1 mM $MgCl_2$, 1 mM EGTA (pH 6.8); C2CF, bis-caged carboxyfluorescein; rf, relative fluorescence.

origin. Approximately 80% of compound 4 was converted to compound 5 by this procedure. The reaction was filtered to remove dicyclohexylurea. It was extracted with two 5-ml portions of diethylether, which formed a two-phase system with the reaction mixture. This concentrated the DMSO phase to 1 ml of dark yellow solution. The product was precipitated from the DMSO phase with 10 ml of ethyl-acetate, collected by filtration, and dried for several days under high vacuum to give 0.7 g of pale brown powder. This workup removed residual dicyclohexylcarbodiimide, which caused extensive tubulin cross-linking if present. Fluorescence spectrometry before and after photolysis suggested that the final product was ~75% pure, but that the contaminants were mostly nonfluorescent. The dry reagent was stored desiccated at −20°C, and was unchanged after several months. Solutions in dry DMSO are also stable at −20°C.

The product and intermediates in this synthetic scheme were characterized by their optical spectra before and after photolysis, and by TLC. All the reactions are well characterized for similar compounds. The synthesis is not fully optimized, but the method above has been repeated three times with a similar yield of useful reagent each time.

Tubulin Labeling

See Table I. 50 μM phosphocellulose-purified bovine brain tubulin (Mitchison and Kirschner, 1984), was stored at −80°C in 80 mM KPipes, 1 mM $MgCl_2$, 1 mM EGTA (pH 6.8) (BRB80). 4 mg for analytical work, or 40 mg for preparative work, was thawed; then glycerol was added to 33% (vol/vol) GTP to 1 mM and $MgCl_2$ to 5 mM. After 20 min at 37°C, the microtubules were layered over 5-ml cushions of 0.1 M Na-Hepes, 1 mM $MgCl_2$, 1 mM EGTA (pH 8.5) containing 60% (vol/vol) glycerol and pelleted at 50,000 rpm, 35°C, 40 min in a rotor (model 50 T; Beckman Instruments, Palo Alto, CA). It was important to use glycerol rather than sucrose in this cushion to stabilize the microtubules at the high pH. After carefully aspirating the supernatant, the pellets were resuspended in a small volume of the cushion buffer containing 40% (vol/vol) glycerol at 37°C. The final tubulin concentration (present as microtubules) was ~500 μM. C2CF-SNHS (compound 5) was dissolved in DMSO (anhydrous sure-seal grade) at 50 mg/ml. 42 μl of C2CF-SNHS solution was added per milliliter of microtubule solution. The reagent was added slowly as it was vortexed to allow thorough mixing. The microtubule solution was returned to 37°C and incubated for 15 min and was vortexed briefly every 3 min. The reaction was terminated and the pH lowered by adding an equal volume of 2× BRB80 containing 0.2 M K-glutamate and 40% (vol/vol) glycerol, and vortexing. After this step, functional labeled tubulin was purified out of the labeling reaction exactly as described for rhodamine-labeling (Kellogg et al., 1988). Briefly, the labeled microtubules were sedimented through a 50% sucrose cushion in BRB80 and depolymerized by incubating at 4°C in BRB80. For C2CF labeling, I usually sonicated the microtubule pellet briefly in the cold buffer, because they were rather resistant to depolymerization immediately after the labeling step. The tubulin solution was sedimented cold to remove denatured protein and free reagent. The soluble tubulin was then polymerized using 1 mM GTP, 5 mM $MgCl_2$, and 33% vol/vol glycerol at 37°C. The microtubules were sedimented through a sucrose cushion again. The depolymerization (no sonication), cold spin, repolymerization, and pelleting through a sucrose cushion were repeated to ensure that the final preparation was fully polymerization competent and free of uncoupled fluorochrome. The final pellet was depolymerized in injection buffer (50 mM K-glutamate, 0.5 mM glutamic acid, 0.5 mM $MgCl_2$), sedimented in an airfuge (Beckman Instruments) for 5 min at 4°C, frozen in 2-μl aliquots using liquid nitrogen, and stored at −80°C. For microinjection experiments the tubulin was thawed, diluted to 50 μM with injection buffer, sedimented at 10,000 rpm, 4°C, 5 min in a microfuge and kept on ice. Aliquots were discarded 2 h after thawing.

The C2CF-labeled tubulin was examined by SDS-PAGE (data not shown) and found to consist of a doublet at 55 kD corresponding to α- and β-tubulin. Microtubule-associated proteins were undetectable by Coomassie blue staining. In early reagent preparations, cross-linked tubulin oligomers were formed due to dicyclohexylcarbodiimide contamination. These were not detected when the reagent was purified as described above. Unbound C2CF was assayed by TLC using system C, which effectively denatures the protein. After development the plates were neutralized in ammonia vapor, photoactivated using 260-nm light, and examined using 360-nm light. Free C2CF runs behind the dye front, whereas labeled tubulin stays at the origin. The final preparation contained some detectable free C2CF, but always <5% of the total fluorochrome.

Determination of Labeling Stoichiometry

Protein concentration was measured using Bradford reagent (Bradford, 1976) and bovine IgG standard. I assumed a molecular mass of 100 kD for the tubulin dimer. C2CF concentration was determined by complete photolysis in a cuvette using a hand lamp (360 nm for 40 min or 260 nm for 10 min). The concentration of the activation product was measured by optical absorbance, assuming $\epsilon = 80{,}000$ based on free fluorescein. This is a relatively high value, greater than published values for fluorescein-protein adducts (Haugland, 1989). For this reason, and because photolysis may not go to completion, stoichiometry figures are a minimum estimate.

Observation of C2CF-labeled Single Microtubules

C2CF-labeled tubulin at 60 μm was polymerized in BRB80 containing 1 mM GTP and 10% DMSO for 20 min at 37°C. The labeled microtubules were diluted 200-fold in BRB80 containing 40% glycerol and examined with a fluorescent photomicroscope using a silicon-intensifier target tube (SIT) video camera on constant gain, mercury arc illumination, and conventional fluorescein filters. For photoactivation after polymerization, the microscope field was briefly exposed to 365-nm light using a Hoechst filter set (Carl Zeiss Inc., Thornwood, NY). For photoactivation before polymerization, a drop of C2CF tubulin was placed on parafilm over a metal block at 0°C, and exposed to a 360-nm hand lamp for 30 min at 0°C. It was then polymerized as above. 5 mM DTT was added to the tubulin monomer before activation; omission of sulfhydryl reagent resulted in a noticeable reduction in the number of microtubules formed.

Optical Apparatus

See Fig. 6. The experiments were performed using a microscope (model IM35; Carl Zeiss, Oberkochen, FRG) equipped with epifluorescence optics and a rotating stage. All filters and mirrors were from Omega Optical (Brattleboro, VT). Photoactivation and fluorescence observation were performed using a 100× neofluor phase 3 objective. Fluorescent and phase-contrast images were collected with an Intensifier silicon-intensifier target (ISIT) camera (Cohu, Inc.; San Diego, CA) operated with manual controls. The video signal was processed using an IVS image processor (Interactive Video Systems, Inc., Concord, MA). Both trans- and epiillumination used 100-W halogen light sources. To minimize photodynamic damage and photobleaching the epi-illumination was controlled by a shutter interfaced to the image processor. The transillumination was controlled manually. It was filtered with reflection and absorption heat filters and a 560-nm bandpass filter that prevented photoactivation by this beam. A phase condenser made by Modulation Optics (Greenvale, NY) allowed phase 3 illumination with 10 mm working distance.

Local photoactivation was achieved using a 365-nm beam directed into the epiillumination tube. The 365-nm beam was generated by a 100-W mercury arc (Oriel Corp., Stamford, CT) filtered through heat adsorbing and colored glass (model UG1; America Glass & Scientific Products, Yonkers, NY) filters and controlled by an electronic shutter (Vincent Associates, Rochester, NY). An adjustable slit (cat. no. 22-8551; Ealing Optical, S. Natick, MA) was positioned so that its image was in the same focal plane as the specimen. The arc lamp was focussed onto this slit using only a condensing lens (cat. no. 467274, Carl Zeiss Inc.) in the lamp housing. Additional focusing lenses did not increase the beam intensity. The beam was introduced into the epiillumination tube on the objective side of the field-diaphram using a dichroic mirror (390-nm long pass) placed in the heat filter position of the tube. Details for the epitube dichroic holder are available on request. The beam was directed up towards the objective and specimen by the fluorescein dichroic mirror in the filter cube (505-nm long pass). The fluorescein excitation filter (485–495 nm) was removed from the filter cube and positioned in front of the light source so as not to block the 360-nm beam. The fluorescein emission filter (505-nm long pass) was situated in the normal filter cube position. This optical configuration had the advantage of not requiring any machining of the microscope itself. The exact position of the slit was crucial in focusing and positioning the photoactivation beam. The slit was imaged by using the 365-nm beam to excite fluorescence in a thin film of a solution of dimethylaminocoumarin (Molecular Probes, Eugene, OR).

Cell Culture

PtK2 cells were obtained from the American Type Culture Collection (Rockville, MD) and grown in F12 medium. LLC-PK1 cells were a gener-

ous gift from Dr. G. Borisy and Dr. V. Centonze (University of Wisconsin, Madison, WI) and were grown in DME-H16 medium. Media were supplemented with 10% FCS, penicillin, streptomycin, and glutamine. Culture was at 37°C in 5% CO_2. For microinjection, cells were plated on untreated glass coverslips. A few hours before the experiment they were transferred to growth medium containing 20 mM Na-Hepes, pH 7.4. They were then mounted in this medium in thermostatted chambers and covered with silicone oil. The bath temperature was maintained at 34°C, so that cells directly above the point of contact with the unheated oil immersion objective were at 30–31°C. This was determined with a microprobe thermocouple thermometer and was highly reproducible in an air-conditioned room. All the experiments were conducted with the cells maintained at 30–31°C. Mitosis is slower at this temperature than at 37°C, but proceeds normally. This temperature was chosen because cells appear to suffer less photodynamic damage at lower temperatures (Schulze and Kirschner, 1988), and because biotin injection experiments indicated that lower temperatures tend to suppress microtubule turnover in the polewards portions of kinetochore fibers (Mitchison, T. J., unpublished results).

Microinjection

Dim incandescent room light was used during needle filling without causing appreciable premature photoactivation. The cells were microinjected as described previously (Mitchison et al., 1986) using low air pressure to prevent tubulin aggregation. The cells were observed by phase contrast with a 40× objective illuminated with 560-nm light during injection. Cells either in, or clearly committed to, mitosis were selected for injection. The needle contained tubulin at a concentration of 50 μM, thus 17 μM labeled subunits. There was considerable variability in injected volume, which I estimate to have been 5–10% of the cell volume. Assuming an intracellular tubulin concentration of 20 μM, the injections resulted in an elevation of total tubulin concentration of 10–25%, and a final label stoichiometry of 0.04–0.07. Cells were injected somewhere between early prophase (nuclear envelope intact, chromosomes starting to condense and nucleolus starting to fragment) and metaphase (all chromosomes aligned at the spindle equator). For prophase and prometaphase injections I waited for metaphase before photoactivating, and for metaphase cells I waited at least 8 min to allow incorporation of labeled tubulin subunits into all spindle microtubules including kinetochore fibers (Mitchison et al., 1986). The results were not affected by the time at which the cell was injected.

Photoactivation and Data Collection

Before photoactivation, the microinjected cell was positioned relative to the irradiation beam by rotating the stage. The photoactivation beam was applied for a period of 0.3–0.9 s, which sufficed to give maximum fluorescence intensity in the center of the irradiated area. Further illumination only served to broaden the activated bar. Fluorescence images were collected as soon as possible after activation, and then at regular intervals. These were usually 1 min apart, but images were sometimes collected more frequently to test for possible photobleaching. The fluorescence images were collected using the ISIT camera set at maximum gain, and the shutter was opened just long enough (0.6 s) to sum 15 video frames at each time point and divide the result by 15 to produce an averaged image. This averaging was necessary to produce a reasonable image from the noisy ISIT output. I was careful to insure that the parameters controlling image brightness (camera gain and black level, illumination level, analog-to-digital and digital-to-analog conversion parameters, etc.) were kept constant throughout one photoactivation run. This allowed me to quantitatively compare relative fluorescent intensities between time points, although the absolute fluorescence intensities cannot easily be determined. Phase-contrast images were recorded before activation and then at irregular intervals. They were collected by manually lowering the accelerating voltage on the ISIT (to increase resolution) and then turning on the transillumination beam. Cells were also observed visually using phase contrast between fluorescence images to determine when they entered anaphase.

Photography and Image Analysis

Figs. 5, 6, and 8 were made by photographing a TV monitor using constant gain, contrast, and film exposure. The prints were made at constant exposure using low-contrast paper to avoid saturation of the image at the early time points.

Line intensity measurements (Fig. 9) were made using Image-1 software (IVS). The poles were located using the background spindle fluorescence. The location of the poles was checked using the phase images, but the fluorescence provided more accurate locations. Five parallel lines were traced from pole to pole and averaged. All scans were normalized to the same length by adding background values equally to the two poles if necessary. If the pole-to-pole difference changed by >10% over the analysis the run was discarded. The preactivation scan was subtracted from the subsequent scans to remove the black-level pixel value, which was ~10 units.

Average intensity in a predefined spindle zone (Fig. 10) was determined only for spindles that moved <1 μm within the cell during a run. A phase image was displayed, and the spindle outline was traced. The spindle outline was divided along its axis into seven rectangular zones of equal length (~2 μm). I did not attempt to use more narrowly defined zones because all spindles moved a little during the runs. The boundary coordinates of a given zone were entered into an image-1 journal that then automatically stepped through a time sequence and determined the mean intensity at each time point in this zone. The advantage of this method is that it is free of potential operator bias because the zones are defined without looking at the fluorescence. Preactivation values were then subtracted from subsequent time points to remove the black-level pixel value as above.

Results

Synthesis of Caged Fluorescein

The structure of the novel photoactivable fluorescein derivative is shown in Fig. 1 *A*. It will be referred to as bis-caged carboxyfluorescein (C2CF). C2CF is nonfluorescent because the fluorescein ring is trapped as its nonfluorescent lactone tautomer. The key reaction in the synthesis of C2CF was the alkylation of both of the phenolic oxygens of the fluorescein ring with *o*-nitrobenzylbromide. The conditions for this reaction were developed by Krafft et al. (1988) to favor the formation of a fluorescein-bis-ether over a fluorescein-mono-ether-mono-ester. Initially I tried reacting fluorescein with the diazo intermediate of Walker et al. (1988), but this led to preferential esterification of the fluorescein carboxy group (data not shown). Fig. 1 *A* also shows the photolysis reaction of C2CF, in which 2 mol of *o*-nitroso-benzaldehyde are released and a carboxyfluorescein derivative is regenerated. The product is drawn as the highly fluorescent carboxylic acid tautomer that predominates in aqueous solution. Because this reaction is well documented for related molecules (Kaplan et al., 1978; McCray et al., 1980; Walker et al., 1988), I have not demonstrated it directly for C2CF. Absorption and fluorescence spectra taken during photoactivation are consistent with this mechanism (see below and Fig. 2 *A*).

The side-chain carboxyl group of C2CF was activated for protein labeling as the *N*-hydroxy-sulfosuccinimide ester (Fig. 1 *B*). *N*-Hydroxy-succinimide esters, which react with proteins by acylation of lysine amino groups, were previously found to be the most useful activated derivatives for tubulin labeling (Kellogg et al., 1988; Sammak and Borisy, 1988). The sulfosuccinimide ester was chosen over the simple succinimide ester because of its greater solubility in aqueous solution (Staros, 1982).

Tubulin Labeling

Modification of tubulin with C2CF was rather difficult due to limited water solubility of the reagent and its hydrolysis product. The pH 6.8 protocols developed for labeling tubulin with *N*-hydroxysuccinimide esters of biotin and rhodamine gave low yields of modified tubulin due to large precipitates of excess reagent. In addition the tubulin became preferentially labeled with a minor fluorescent contaminant in the reagent preparation, probably because it was more water soluble than C2CF. Thus, I developed the pH 8.5 labeling

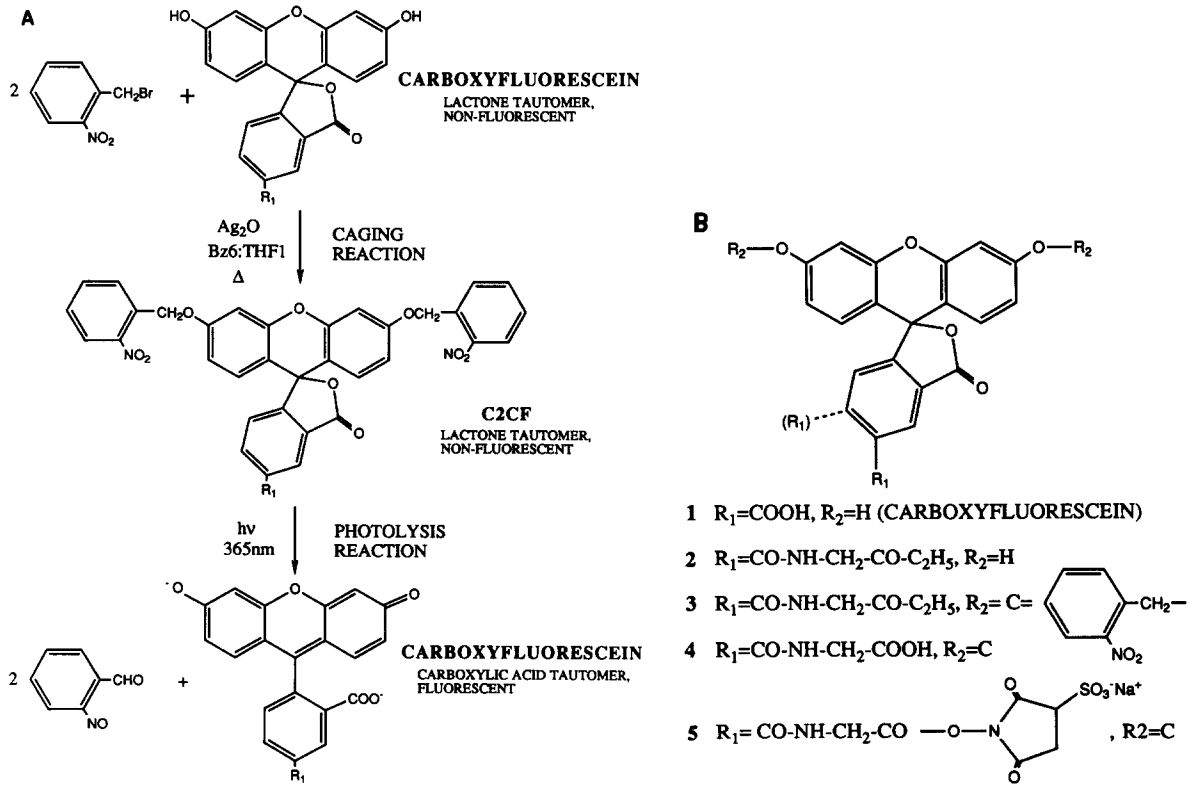

Figure 1. (*A*) Caging and photoactivation reactions of C2CF. Carboxyfluorescein, drawn as its nonfluorescent lactone tautomer, reacts with *o*-nitrobenzylbromide to give C2CF. When this is illuminated at 365 nm, the cage groups are efficiently cleaved off as *o*-nitrosobenzaldehyde. Carboxyfluorescein, drawn as the fluorescent carboxylic acid tautomer, is regenerated. (*B*) Intermediates during C2CF synthesis.

protocol described in Materials and Methods. It reproducibly gave yields of 15–25% and a labeling stoichiometry of 0.3–0.4 C2CF molecules per tubulin dimer (Table I). This procedure may be useful for labeling tubulin with other lysine reactive probes for which elevated pH promotes coupling.

Labeled Tubulin: Photochemical Properties

The optical absorbtion of the C2CF-labeled tubulin before and after photoactivation are shown in Fig. 2 *A*. Before activation, there was no detectable visible absorbance as expected for the lactone form of fluorescein (Miller, 1983; Haugland, 1989). During activation by 360-nm light, the first visible light adsorbing species to be formed had two absorbtion peaks at 460 and 480 nm. This spectrum is characteristic of fluorescein mono-ethers and fluoresceins protonated on the phenolic oxygen (Miller, 1983; Babcock and Kramp, 1983). The transient appearance of a mono-ether intermediate indicates that the two caging groups are photolyzed independently. As the reaction continues, the absorp-

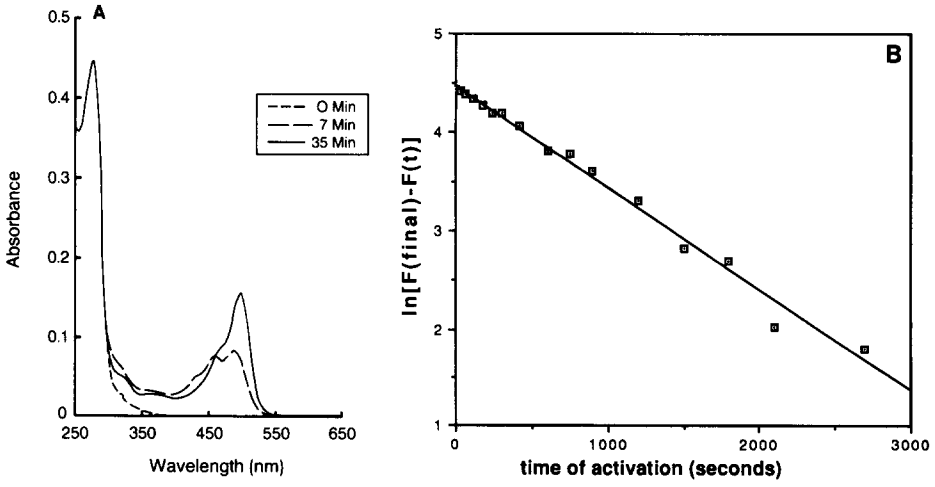

Figure 2. (*A*) Optical spectrum of C2CF tubulin (5.5 μM in 0.1 M $NaHCO_3$) before and after exposure to 360-nm light for the indicated times. The 7-min spectrum shows two peaks, which is characteristic of a fluorescein mono-ether. (*B*) Fluorescence yield of C2CF tubulin as a function of time during photoactivation with a 360-nm hand lamp. Fluorescence measured with a spectrofluorimeter. Excitation, 490 nm; emission, 522 nm. This graph is plotted as ln (final fluorescence yield − fluorescence yield at time *t*). The line is a linear least squares fit to the points. The close fit indicates that acquisition of fluorescence behaves as a simple first-order reaction. The actual values of fluorescence emission were: 0 min, 0.26; 60 min, 100.0 (arbitrary units).

Table I. Preparation of C2CF-labeled Tubulin

	Total protein	Yield	Label stoichiometry
	mg	*%*	*mol C2CF/dimer*
Starting material	4.0		
pH 8.5 pellet	3.7	92	
1st labeled warm pellet	3.7	92	
1st cold supernatant	2.3	57	
2nd cold supernatant	1.3	32	0.34
3rd cold supernatant = final	0.84	21	0.34

Yields and labeling stoichiometries during the preparation of C2CF-labeled tubulin.

Table II. Polymerization Competence of C2CF-labeled Tubulin under Stringent Conditions

	Total protein	Protein yield	Label stoichiometry	Label yield
	mg	*%*	*mol C2CF/dimer*	*%*
Initial mixture	0.55		0.053	
Final mixture	0.20	36	0.043	29

The polymerization competence of C2CF tubulin was determined in BRB80 without glycerol or DMSO. The initial mixture was C2CF tubulin diluted sixfold with unlabeled tubulin. Polymerization was initiated by adding microtubule seeds. After 20 min, the microtubules were sedimented through a sucrose cushion, cold depolymerized, and sedimented cold to give the final mixture.

tion spectrum changes to the single sharp peak at 498 nm characteristic of carboxyfluorescein (Babcock and Kramp, 1983).

The fluorescence yield of C2CF-labeled tubulin during photoactivation is shown in Fig. 2 *B*. The final fluorescence was at least 300-fold greater than the initial. The appearance of fluorescence during activation showed simple first-order kinetics. This, combined with the rapid generation of the two-peaked spectrum, probably indicate that loss of the second caging group is slower than loss of the first one. I have not attempted to determine the quantum efficiency of photolysis, which has been reported to be ~0.3 per cage group for similar compounds (Krafft et al., 1988). Fully activated, C2CF-labeled tubulin had a fluorescence spectrum typical of a protein-fluorescein conjugate (Haugland, 1989), with maximal excitation at 498 nm, and emission at 522 nm. When normalized to absorption, the fluorescence yield of fully activated C2CF tubulin was 33% of that of free sodium fluorescein (excitation, 488 nm; emission, 512 nm). Because fluorescein has a quantum yield of fluorescence close to 1.0, the quantum yield of activated, C2CF-labeled tubulin is ~0.3, quite reasonable for a protein adduct (Haugland, 1989).

Labeled Tubulin: Functional Properties

C2CF-labeled tubulin was purified by two cycles of warm polymerization and cold depolymerization (see Materials and Methods), thus selecting for polymerization-competent subunits. The second cycle of polymerization in glycerol containing buffer gave a good (65%) yield of protein and little change (0–10% decrease typical) in labeling stoichiometry (Table I). This indicates that most of the free dye and inactivated subunits are removed during the first cycle and that labeled and unlabeled subunits polymerize equally well in the second cycle.

To determine whether C2CF-labeled tubulin is able to polymerize under conditions more similar to those inside cells, I mixed labeled and unlabeled tubulin to a final label stoichiometry similar to that present in microinjected cells (sixfold dilution of the labeled preparation, final stoichiometry 0.053/dimer). This mixture was then polymerized in Pipes buffer without glycerol or other additives by adding short microtubule fragments to nucleate polymerization. One cycle of warm polymerization, sedimentation through sucrose, and cold depolymerization under these conditions resulted in a 36% recovery of total tubulin, compared with 60–80% recovery in glycerol buffers. The recovery of fluorochrome, determined by photoactivation before and after the cycle, was 29% (Table II). This slight discrimination against labeled subunits could reflect a slightly lower affinity for the polymer lattice or a higher tendency to denature. When tubulin is polymerized without glycerol or microtubule-associated proteins, there is a high fraction of so-called "noncompetent" protein, despite the fact that much more would polymerize if glycerol were added. When the steady-state monomer concentration is determined under these conditions, the slope of the polymer as a function of monomer has a slope of <1 (Mitchison and Kirschner, 1984). This explains the low total protein recovery in the assay, but the reason for this high proportion of apparently inactive subunits is not known.

I first used fluorescence microscopy to determine whether C2CF-labeled tubulin polymerizes into normal microtubules. A field of microtubules polymerized from C2CF-labeled tubulin is shown in Fig. 3, *A* and *B*, before and after photoactivation. The microtubules that became visible appeared completely normal. Compared with a similar concentration of unlabeled tubulin, the C2CF-labeled protein made more microtubules of shorter length, indicating that the label promotes microtubule nucleation. Photoactivation of labeled tubulin monomers did not prevent their subsequent polymerization, as shown in Fig. 3 *C*, provided 5 mM DTT was present during activation. Sulfhydryl reagents have been shown to protect proteins during related photocleavage reactions, presumably by scavenging the reactive *o*-nitrosoaldehyde product (Kaplan et al., 1978; Walker et al., 1988). Within the cell, glutathione and other nucleophiles should fulfill this role. C2CF microtubules were also observed by negative stain microscopy (Fig. 4). They appeared identical in structure to microtubules polymerized from unlabeled tubulin. I noticed a higher proportion of sheets and other unrolled structures in the labeled microtubules, but this difference disappeared when the labeled protein was diluted threefold or more with unlabeled protein.

Because of concern in the literature that photochemical reactions may damage microtubules, I tested whether photoactivation of C2CF microtubules caused observable breakage. Microtubules were polymerized containing both C2CF- and rhodamine-labeled subunits (Fig. 5). The rhodamine allowed me to determine microtubule length before photoactivation. I noticed no detectable breakage due to photoactivation in BRB80 containing taxol but no photoprotecting reagents. Prolonged illumination by fluorescein excitation light caused photobleaching, and this did cause occasional breaks as reported (Vigers et al., 1988). Thus, under conditions where photobleaching can cause microtubule breakage, pho-

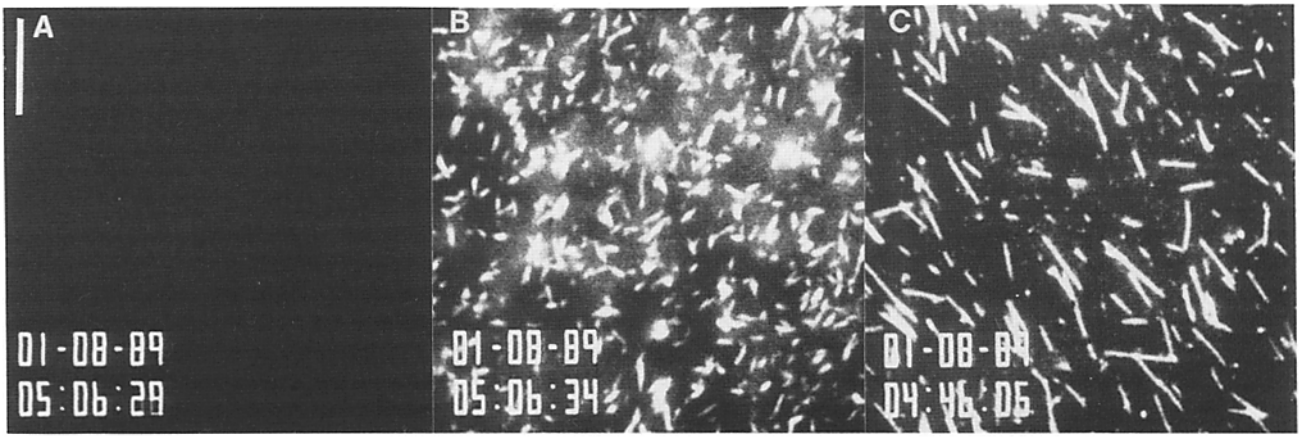

Figure 3. Fluorescent images of C2CF-labeled microtubules before and after photoactivation. Images were recorded with a SIT video camera using standard fluorescein filters. A photograph of part of the video monitor is shown. (*A*) C2CF-labeled microtubules before activation. (*B*) The same field of C2CF labeled microtubules after activation using 1 s of exposure to the filter set (Hoechst) (excitation, 365 nm). (*C*) Microtubules polymerized using the same concentration of C2CF tubulin as in *A* and *B*, except that it was preactivated before polymerization. By eye, fields like *A* were quite dark, and fields like *B* and *C* showed bright green microtubules, which bleached rapidly in the illumination beam. Bar, 10 μm.

toactivation does not. I should emphasize that this experiment used a much higher illumination intensity, and a higher labeling stoichiometry, than the in vivo experiments. I saw rather little breakage induced by photobleaching, and I doubt that microtubule damage influenced the behavior of activated zones in vivo.

Spindle Microtubule Dynamics in Vivo

Two cell lines were used for this study: PtK2 (potoroo kidney, 14 chromosomes) and LLC-PK1 (pig kidney, 38 chromosomes). These epithelial lines were chosen because they remain flat during mitosis. Cells were injected with C2CF-labeled tubulin between early prophase and metaphase, and sufficient time was allowed before photoactivation for all spindle microtubules to incorporate label. I estimate that the injections resulted in ~1 subunit in 15 in the cell being labeled, and an elevation of total tubulin concentration of 10–25% (see Materials and Methods). Successful injection of C2CF-labeled tubulin did not affect progress through mitosis in either line. PtK2 cells in older cultures sometimes exhibited dissolution of the spindle after injection, but this was also observed with buffer injections. LLC-PK1 cells were generally more robust and tolerant to injection. Time-lapse observations showed that cells injected in prophase, before nuclear envelope breakdown, made spindles and progressed into anaphase within the normal time range, which was rather variable in these lines (nuclear envelope breakdown: metaphase, 10–30 min; metaphase, 10–30 min; anaphase, 5–10 min). Injected cells exhibited prometaphase and anaphase chromosome movement rates that were as fast as control cells. To restrict the analysis to normally functioning spindles, I have only analyzed data from cells that proceeded into anaphase after observation in metaphase.

Once an injected cell reached metaphase, its spindle was locally activated by irradiation for 0.3–0.9 s with a 365-nm microbeam to form a bar of fluorescence across the spindle. Subsequently it was observed with a low level of 490-nm light illuminating the whole field, to follow the movement of the fluorescent molecules. The optical apparatus used is diagrammed in Fig. 6 and described in Materials and Methods. Before activation, the fluorescent image was essentially dark; occasionally a faint outline of the spindle was visible in heavily injected cells. The slit irradiation generated a bar of fluorescence across the spindle (Figs. 6 and 7). The slit was aimed at a position between the chromosomes and the poles. With optimal focussing of the slit, the initial fluorescent bar had an apparent width at half intensity of 1.5–2.5 μm. The ISIT camera at full gain produces considerable broadening of a bright bar, and tests at lower gain suggested that the true width of the activated zone was ~1 μm.

When cells were imaged within a few seconds of activation

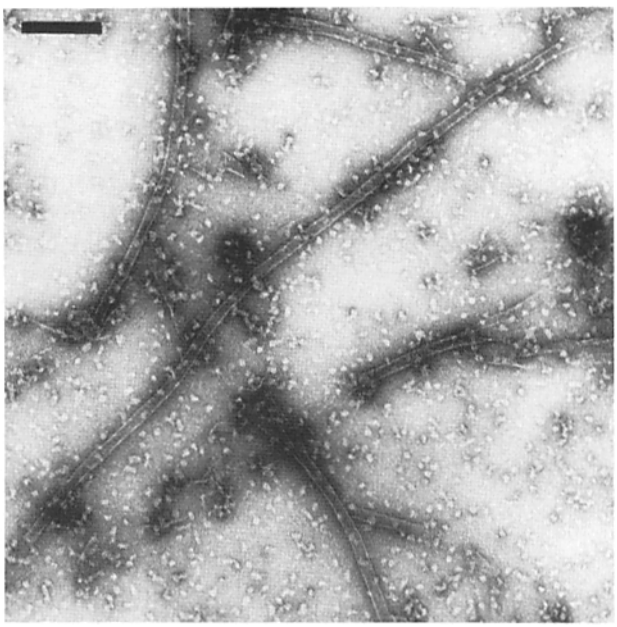

Figure 4. Negative-stain electron micrograph of C2CF microtubules. Labeled tubulin was polymerized in BRB80 containing 1 mM GTP, and the microtubules were stained with 1% uranyl acetate. Bar, 0.2 μm.

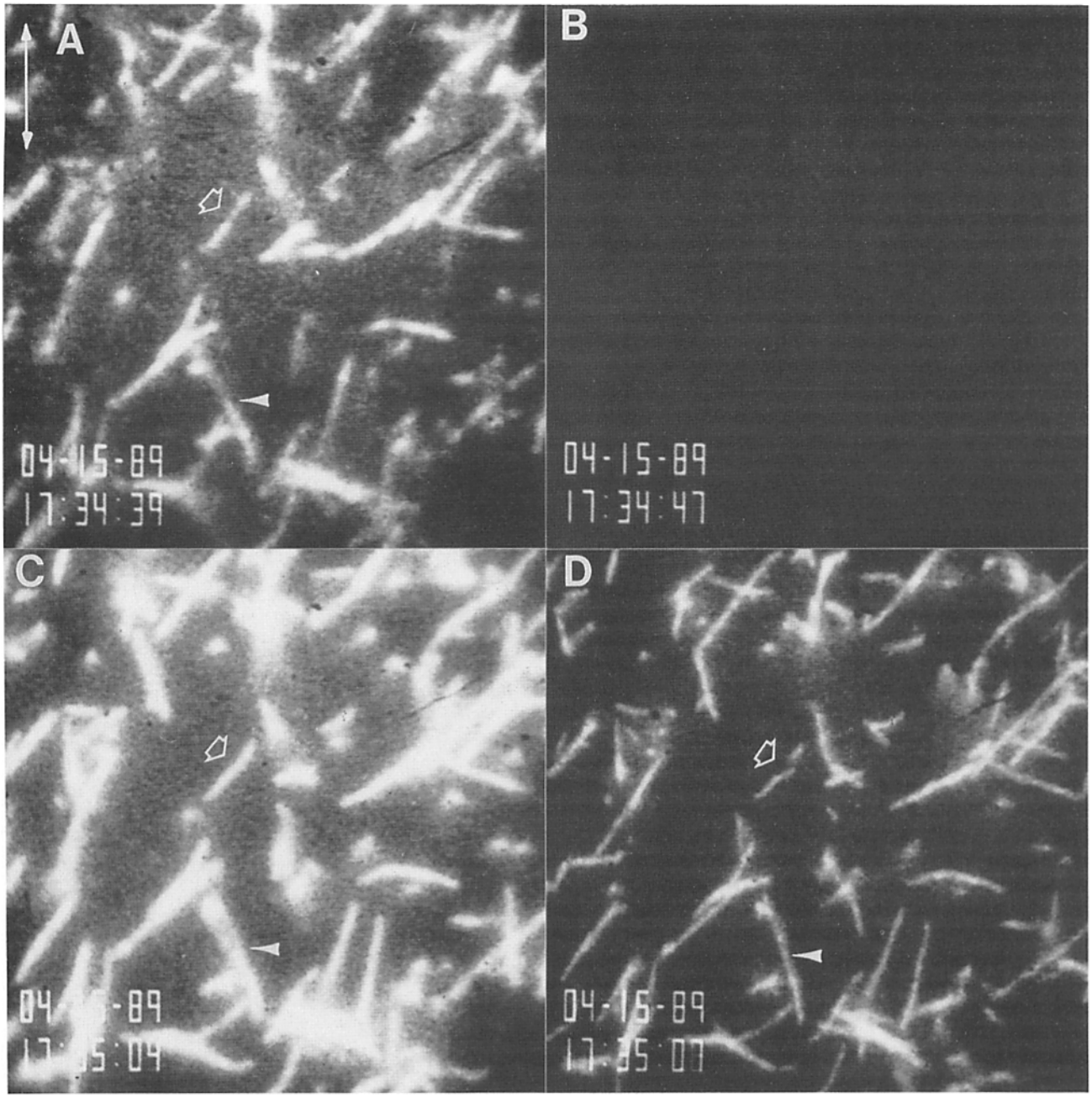

Figure 5. Photoactivation does not cause microtubule breakage. Microtubules were polymerized from C2CF-labeled tubulin, mixed with a small amount of X-rhodamine-labeled tubulin (made using the high pH protocol described in the Materials and Methods), and polymerized in BRB80 containing 1 mM GTP. After polymerization, the microtubules were diluted in BRB80 containing 10 μM taxol for observation. The microtubules contained approximately one subunit in three labeled with C2CF and one subunit in ten labeled with X-rhodamine. All four panels show the same microscopic field viewed with the ISIT video camera, using mercury arc illumination and a fluorescence photomicroscope. The first panel (*A*) shows the labeled microtubules in the rhodamine channel. The subsequent images (*B–D*) show the microtubules in the fluorescein channel. *B* is before, and *C* and *D* are after photoactivation as per Fig. 3. The last two frames were after 2- and 5-s exposures to excitation light (450–490 nm), respectively. Considerable photobleaching is apparent in *D*. Photoactivation did not cause microtubule breakage, even to microtubules which were not attached to the coverslip. However, prolonged exposure to the high-intensity fluorescein excitation beam did cause occasional breaks (*open arrow*). Bar, 5 μm.

the fluorescent bar usually exhibited bright, uniform intensity (Figs. 7 and 8, *3 s*). After 30–90 s it lost intensity and became less uniform. In PtK2 spindles, the bar usually resolved into a number of distinct fluorescent streaks parallel to the spindle axis (Fig. 7, *92 s*), presumably corresponding to marked zones on individual kinetochore fibers. This was not observed in the LLC-PK1 spindles, which have more kinetochore fibers with fewer microtubules in each one (Fig. 8, *169 s*). As the initial fluorescent bar dimmed, the whole spindle became slightly more fluorescent, probably because

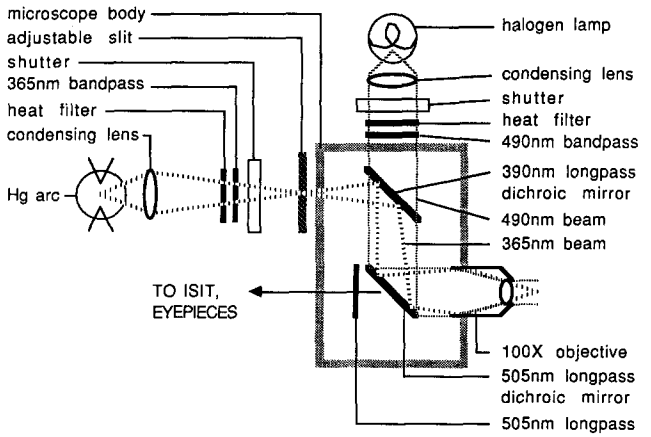

Figure 6. Diagram of the optical apparatus used for local photoactivation of fluorescence in living cells. See Materials and Methods for details.

activated monomers diffuse away from the initial zone, and then polymerize into microtubules throughout the spindle. This increase in spindle background fluorescence allowed me to determine the position of the spindle poles, which was confirmed by comparison with phase-contrast images. Activation of a large region of the cell using multiple pulses at 365 nm produced a fluorescent spindle appearing very similar to published reports where fluorescein-labeled tubulin was injected (Saxton et al., 1984) (not shown).

After the initial dimming, fluorescence in the activated region decreased more slowly. Over a period of minutes, the fluorescent zones moved towards the proximal pole (Figs. 7 and 8). The intensity of the marked zone decreased as it moved polewards, but it remained much brighter than the background spindle fluorescence. This can be appreciated by comparing the fluorescence intensity of the activated half-spindle to that of the unactivated half-spindle. The polewards movement resulted in fluorescence accumulating at the spindle pole (Fig. 7, *1,021 s*; Fig. 8, *774 s*), and eventually disappearing, leaving homogeneous weak fluorescence over the spindle. In some PtK2 spindles, individual fluorescent zones could be observed to move polewards at different rates. This was clearest in time-lapse movies following activation, but it can be seen in Fig. 7. At 618 s, note how the most central fluorescent stripe has moved polewards more slowly than the stripes above it.

Polewards movement of fluorescent zones occurred throughout metaphase, and frequently the cell entered anaphase while a marked zone was proceeding polewards. Fig. 8 shows a sequence in which a mark was generated with the chromosomes still loosely congressed. This mark moved all the way to the left pole. A second mark was then generated on the right half spindle, and this moved to the right pole before the cell entered anaphase. The rate of polewards movement was similar in each case. Generally, cells did not remain in metaphase long enough to perform such double-marking experiments, but comparison of many cells suggests that flux occurs at similar rates throughout metaphase.

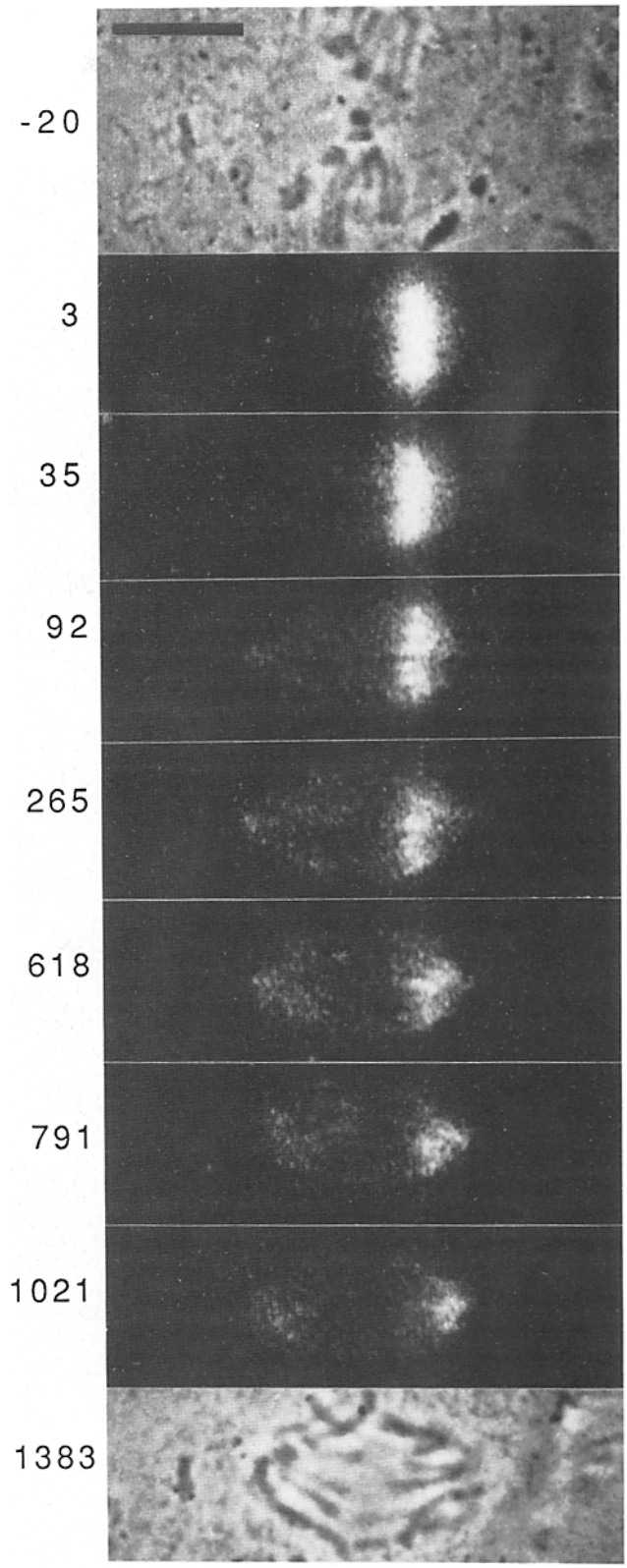

Figure 7. Photoactivation run in a PtK2 cell. Selected shots from the time-lapse record. The times given are in seconds relative to the photoactivation pulse. Phase-contrast images are shown at −20 (metaphase) and 1,383 s (anaphase). The cell entered anaphase at ~1,100 s. The remaining images are fluorescent. The preactivation shot was almost dark and is not shown. The initial fluorescent bar (*3 s*) resolves into zones probably corresponding to individual kinetochore fibers by 92 s. The individual fluorescent zones move polewards at different rates. Note how the centermost zone lags relative to the two upper zones at 618 s. Bar, 10 μm.

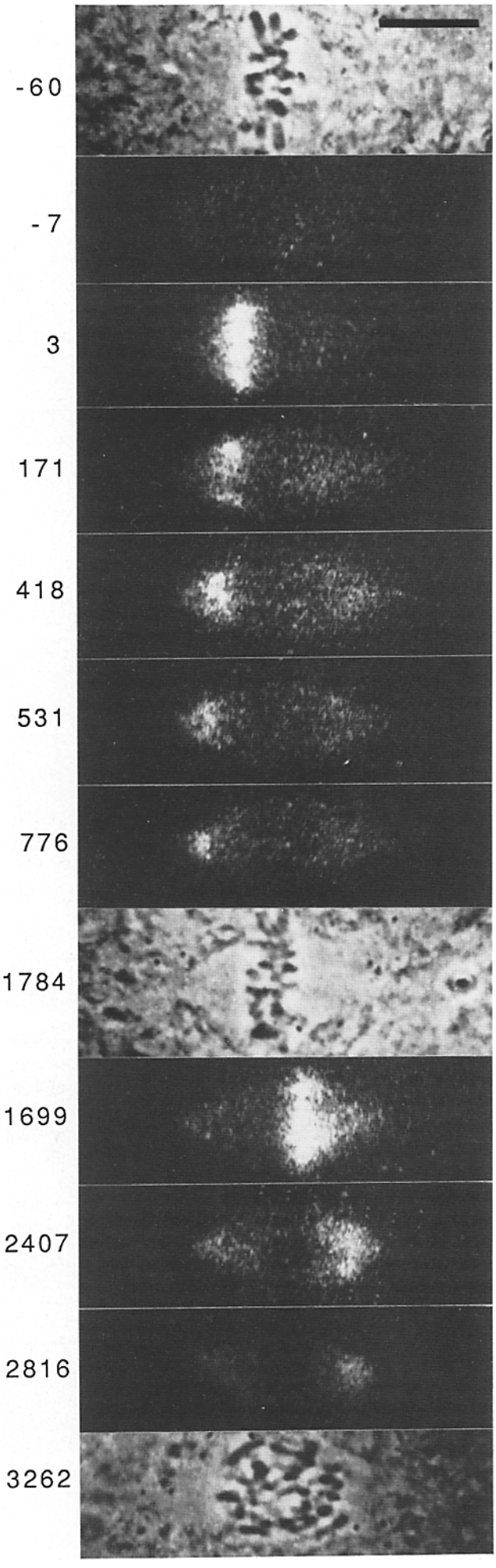

To quantitate the polewards movement of fluorescence, I measured the brightness of the image along a line between the two spindle poles at different times after activation (Fig. 9). To reduce the noise, five parallel lines one pixel apart were averaged, corresponding to an 0.8-μm-wide strip. Although this procedure only follows the movement of a small part of the initial fluorescent bar, it has the advantage of following fluorescence over the whole spindle. The unirradiated half-spindle becomes slightly fluorescent because of diffusion and polymerization of activated monomer. By comparing the two halves, this diffusional component can be distinguished from any vectorial movement of microtubule polymer. This quantitation method bears out the visual impression. After photoactivation, a distinct peak of label can be seen, which broadens and moves polewards with time. It is important to note that progressively more polewards regions actually increase in intensity with time, so I can rule out the possibility that the impression of movement is generated simply from selective loss of fluorescence at the equator. Fig. 9 shows the result from a single cell (the one in Fig. 8); similar results were obtained from other cells.

One reservation about the quantitation procedure in Fig. 9 was potential uncertainty in determining the position of the spindle poles from the weak spindle background fluorescence. As an alternative method, fluorescence intensity was determined as a function of spindle position by an automated procedure which used the phase-contrast image as a reference (Fig. 10, see Materials and Methods). This procedure was only applicable to spindles which did not move around within the cell. Compared with the procedure in Fig. 9, it was less useful for determining the rate of movement of fluorescence, but has the advantages of measuring total fluorescent intensity, and of avoiding any possibility of operator bias. With time, successive areas poleward of the initially activated zone gained fluorescence intensity, whereas the initially activated area lost intensity. This vectorial movement of fluorescence indicates that marked zones on microtubules were moving polewards. The total amount of localized fluorescence at each position as a function of time was estimated by multiplying the average intensity in each zone by its area, and then normalizing to the fluorescence in zone 5 at 5 s. Calling this initial fluorescence 100%, the amount in the same zone at 35 s was 44%, the amount in zone 6 when it was maximally labeled at 254 s was 26%, and the amount in zone 7 at 674 s was 14%. This quantitation is approximate because of uncertainties in the linearity of the detection system, and contributions from out of focus information. Similar results were obtained from two other runs analyzed in this way.

Polewards movements of fluorescent zones was a consistent observation. The most recent 42 runs (35 PtK2, 7 LLC-

Figure 8. Photoactivation run in an LLC-PK1 cell. Selected shots from the time-lapse record. Time is given in seconds relative to the first photoactivation pulse. Phase-contrast images are shown at $t = -60$ (early metaphase), 1,784 (mid-metaphase), and 3,262 s (mid anaphase). The remaining images show fluorescence. The same spindle was activated twice: first to the left of the chromosomes at $t = 0$, and later to the right at 1,690 s. In both cases the marked zone proceeded polewards, taking 10 min to reach the pole. Anaphase started after the second pulse had reached the right pole. Bar, 10 μm.

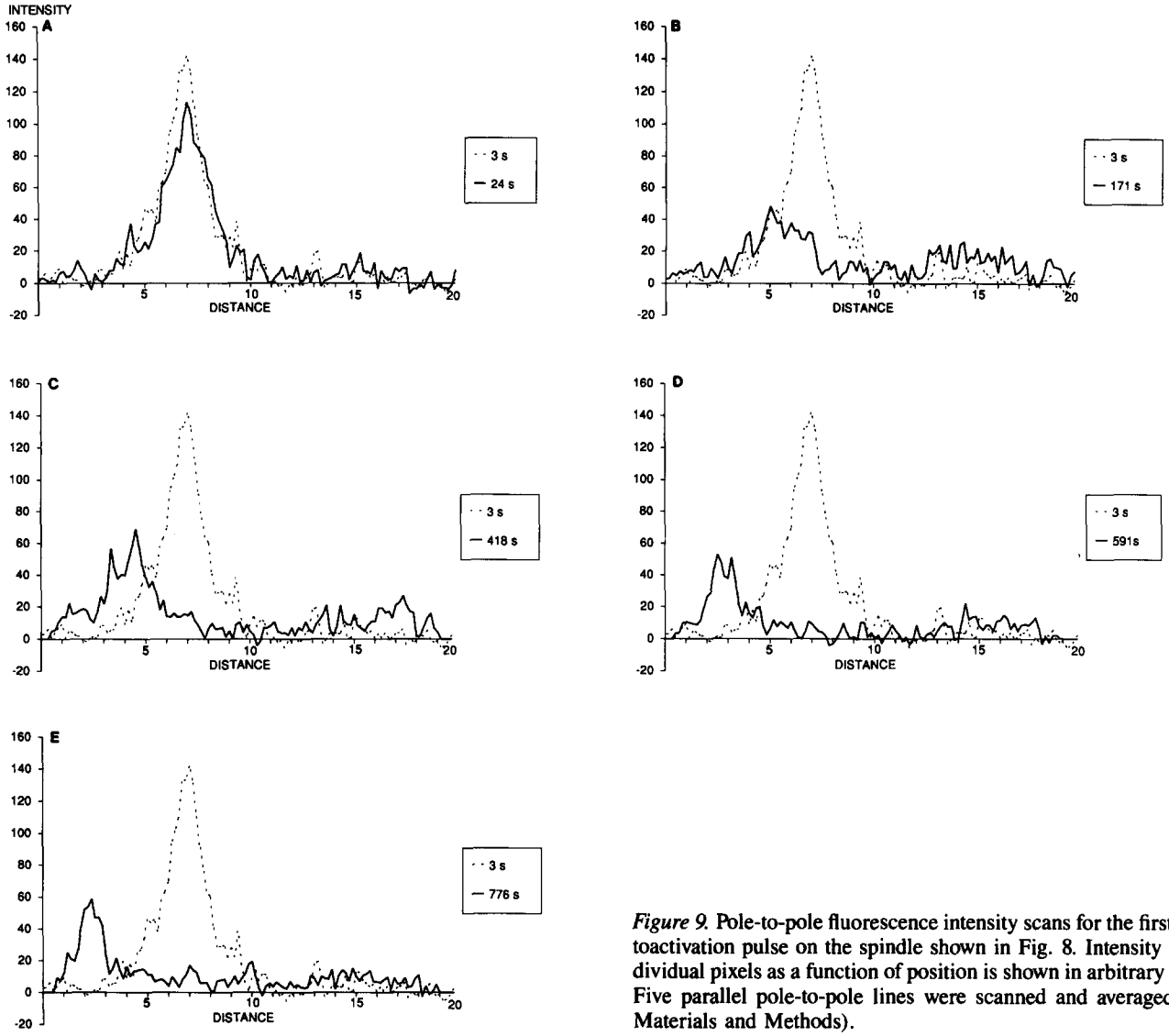

Figure 9. Pole-to-pole fluorescence intensity scans for the first photoactivation pulse on the spindle shown in Fig. 8. Intensity of individual pixels as a function of position is shown in arbitrary units. Five parallel pole-to-pole lines were scanned and averaged (see Materials and Methods).

PK1) were divided into the following categories upon analysis. (*a*) Polewards movement observed and quantitated by the methods of Figs. 7 and 8: 15/42 = 36%. (*b*) Polewards movement observed from time-lapse movies only: 13/42 = 31%. (*c*) No evidence for polewards movement, labeled zone simply disappears: 5/42 = 12%. (*d*) Cell enters anaphase too quickly to analyze movement: 9/42 = 21%. No evidence was seen for movement of labeled zones towards the equator.

To determine the rate of polewards movement of fluorescence, I plotted the position of peak fluorescent intensity against time (Fig. 11). The error bars give a measure of peak width, which made it difficult to determine the movement rate accurately. For the spindle in Figs. 6 and 7, the rate of movement was ~0.39 μm/min, averaged over 5 μm of movement. The first 2.5 μm of movement seemed faster, 0.65 μm/min. Given the width of the fluorescent zones this difference is not necessarily significant, but it probably indicates heterogeneity in movement rates, either with position in the spindle or with time. From this procedure and from direct measurement on a TV monitor, I determined movement rates for 12 PtK2 cells (mean rate, 0.6 μm/min; range, 0.3–1.2) and 3 LLC-PK1 cells (mean rate, 0.5 μm/min; range, 0.4–0.7).

For comparison with the rate of polewards fluorescence movement, I measured the rates of three types of chromosome movements in these cells under the experimental conditions. Measurements were made in uninjected cells using time-lapse, phase-contrast observation, but all three types of movement occurred at similar rates in injected cells. (*a*) Congression to the metaphase plate (highly variable, often discontinuous) = 0.3–5.0 μm/min. Typically, the first chromosomes to congress did so by a series of rapid jumps, whereas later ones moved much more slowly and continuously. (*b*) Metaphase oscillations over the central 10–30% of spindle length (variable, discontinuous) = 1–3 μm/min. In PtK2 cells, these oscillations occurred with equal amplitude and rate right up to anaphase onset. In LLC-PK1 cells, they gradually decreased in amplitude, but not rate, during metaphase. (*c*) Anaphase chromosome to pole movement (constant, continuous) = 2 ± 0.5 μm/min. The nature and rates of these movements are similar to those previously reported (Roos, 1976; Bajer, 1982).

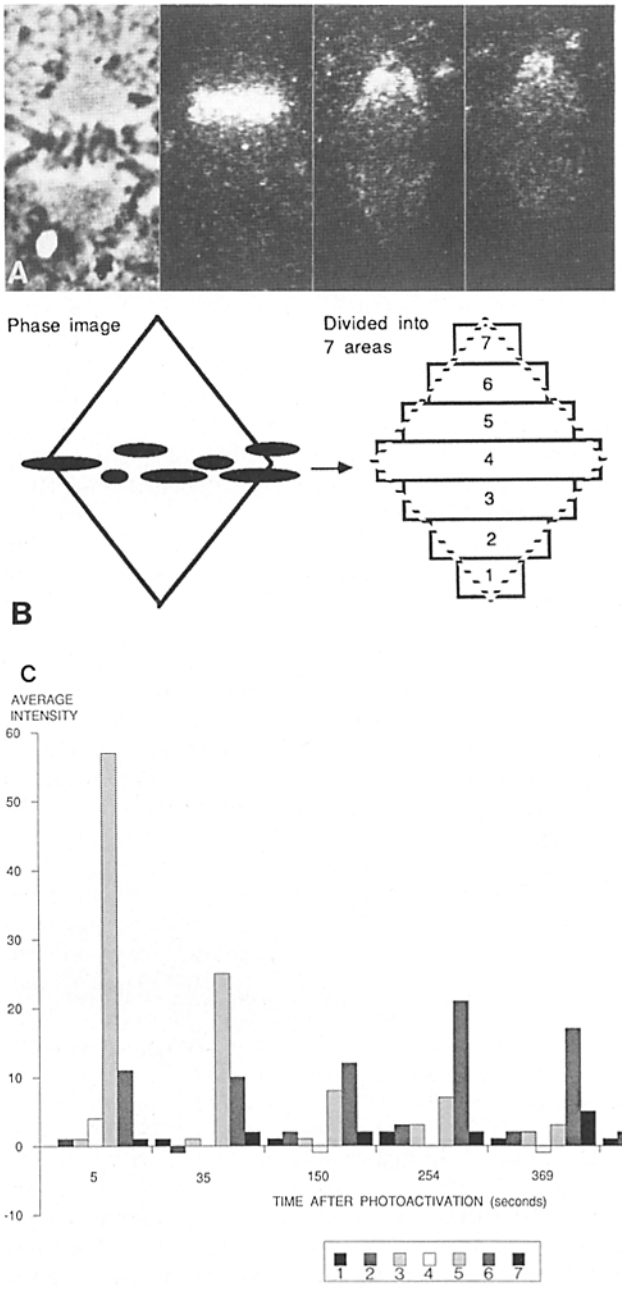

Figure 10. (*A*) Mean fluorescence intensity (arbitrary units) in predefined zones of an LLC-PK1 spindle at different times after photoactivation. Phase-contrast and three fluorescence images of the cell to be analyzed. Times relative to photoactivation are (from left to right): 418, 5, 429, 674 s. Pole to pole distance = 18.8 μm. (*B*) Diagram illustrating how seven zones were drawn on the phase image of the cell. Each zone is 2.7 μm long in the spindle axis. (*C*) Each set of seven bars shows the average fluorescence intensity in successive zones at a given time point, calculated using an automated procedure (see Materials and Methods). The seven time points are a subset of 15 recorded on this cell. Note how the fluorescence intensity in zone *5*, where the activation pulse was delivered, decreases with time. Zone *6* increases at the expense of *5*, and then decreases, and zone *7* later increases at the expense of *6*. This indicates progressive polewards movement of fluorescence intensity.

Discussion

Photoactivation of Fluorescence as a Probe for Microtubule Movement

The initial goal of this project was to develop a photoactivation probe for labeling tubulin. To be useful, such a probe molecule must fulfill six requirements discussed below:

(*a*) *Stably nonfluorescent inside cells.* C2CF is completely nonfluorescent in principle, because the lactone tautomer of fluorescein has no visible absorbance or fluorescence (Miller, 1983). In practice, C2CF-labeled tubulin was almost nonfluorescent, and its fluorescence yield increased at least 300-fold after activation (Fig. 2). The very low level of fluorescence present in unactivated, labeled tubulin is most likely due to a contaminant in the reagent. C2CF is chemically stable inside living cells and it is also unaffected by the 490-nm observation light used to follow activated molecules. This was evidenced by the absence of progressive increase in fluorescence in injected cells exposed only to 490-nm light. In preliminary experiments, dextran labeled with C2CF injected into *Drosophila* embryos remained nonfluorescent, but photoactivable, for at least 18 h (Goetz, E. J., and T. J. Mitchison, unpublished observations). Preliminary experiments using much higher light intensity suggested that 490 nm light may cause very slow photoactivation, but the product is photobleached more rapidly than it is generated.

(*b*) *Ready photoactivation to a stable, highly fluorescent form.* The product of C2CF photoactivation is carboxyfluo-

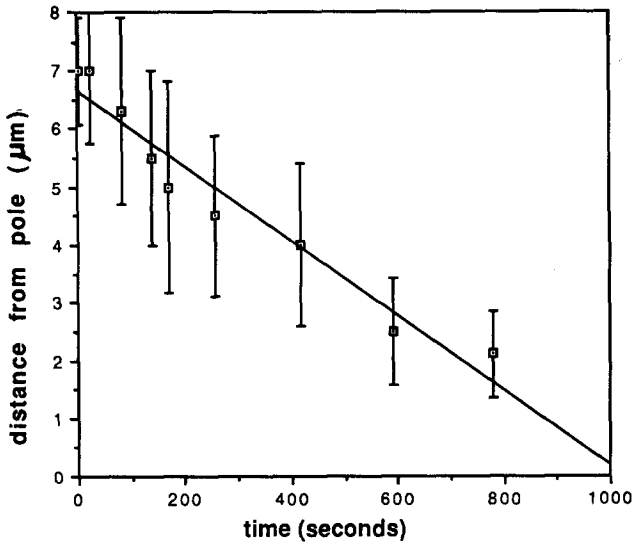

Figure 11. Rate of polewards movement of fluorescence for the cell shown in Fig. 8. The position of maximum fluorescence intensity was determined from the data in Fig. 9 (and other scans, not shown), after smoothing the intensity scans. Error bars are an estimate of the width at half-height of the fluorescent zone. Distance is from the pole closest to the photoactivation bar. The line is a least squares fit through all the points. It gives a polewards movement rate of 0.39 μm/min. A least squares fit through the first six points gave a better linear fit, with a rate of 0.65 μm/min.

rescein attached by a short spacer arm to the protein. Carboxyfluorescein adducts have been widely used for following labeled molecules inside cells. Fluorescein derivatives have high absorption coefficients (ϵ = 80,000) (Haugland, 1989), and good quantum yields of fluorescence, determined as ~0.3 for activated C2CF on tubulin. The main disadvantage of fluoresceins are their propensity for photobleaching and photodynamic damage. In this respect a photoactivable rhodamine would have been preferable, but the *o*-nitrobenzyl-ether chemistry is not readily adaptable to the substituted nitrogen atoms of the useful rhodamines.

(*c*) *Efficient photoactivation by light at a wavelength that does not perturb biological structures.* C2CF was completely activated in a small area by exposure for <1 s to 365-nm light from a mercury arc lamp. Shorter wavelengths would photoactivate even more efficiently, but would be more likely to damage biomolecules; 365-nm light is relatively benign to biological specimens (Hiramoto et al., 1984). Photoactivation caused no detectable microtubule breakage in vitro, even under conditions where photobleaching did (Fig. 5). The photoactivation beam produced no detectable adverse consequences for injected or uninjected cells. The effectiveness of relatively low light doses, despite the low absorption coefficient of the *o*-nitrobenzyl chromophore, stems from the remarkably high quantum efficiency of photocleavage of ether bonds to these caging groups (Kaplan et al., 1978; Krafft et al., 1988).

(*d*) *Ready coupling to proteins.* C2CF was only coupled to tubulin with some difficulty, and the final labeling stoichiometry (0.35/dimer) was lower then optimal. These problems result from the hydrophobic nature of C2CF, which makes it rather insoluble in aqueous solution. The water solubility of the core molecule was enhanced by the highly polar sulfosuccinimide leaving group, allowing a reasonable reaction with tubulin under improved, high pH labeling conditions.

(*e*) *No perturbation to the function of the carrier protein.* In vitro, the ability of the labeled protein to participate in a round of temperature-dependent polymerization and depolymerization was unaffected in a glycerol-containing buffer (Table I), and only slightly depressed under stringent conditions (Table II). C2CF did promote microtubule nucleation (Fig. 3), indicating that the labeled protein is not completely normal. In vivo-labeled tubulin incorporated into spindles without perturbing their function. In preliminary experiments, C2CF-labeled tubulin incorporated into individual interphase microtubules with normal kinetics (Reinsch, S., unpublished observations) and persisted in functional form for 2 d in frog embryos without perturbing development (Reinsch, S., unpublished observations). Although C2CF tubulin is not identical to unlabeled tubulin in its in vitro behavior, it copolymerizes well with normal tubulin, and when diluted by the cellular pool, the properties of the microtubules should be dominated by the majority unlabeled subunits. Thus, I am confident that the distribution and dynamics of C2CF-labeled tubulin faithfully reflect the properties of the total tubulin pool, and that microtubule dynamics are similar in injected and uninjected cells. Probably the highest potential for perturbing labeled microtubules comes from observation of the activated form of C2CF with 490-nm light. Irradiation of fluorescein-labeled proteins can potentially lead to photodynamic toxicity and microtubule breakage (Vigers et al., 1988; Fig. 5). I tried to limit these effects by using a low-level, carefully shuttered light source to excite fluorescence, and a highly sensitive video camera to record emission. I noticed no difference in results from cells whose exposure to 490-nm light varied by at least a factor of five. Finally I analyzed data only from cells which completed mitosis normally, which presumably requires that most of the activated microtubules remain intact.

(*f*) *Side product(s) of activation must be nontoxic to the cell and nonperturbing to the carrier molecule.* The nitrosobenzaldehyde released by photoactivation is potentially toxic, but it is efficiently scavenged by sulfhydryls (Kaplan et al., 1978; Walker et al., 1988), and probably other nucleophiles inside cells. The micromolar levels released in these experiments appear to have caused no detrimental effects on injected cells.

C2CF-labeled tubulin reasonably fulfills all these requirements, and provides a powerful new tool for following the movement of microtubules inside living cells. C2CF should be widely useful for labeling other proteins as well. Photoactivation of fluorescence provides a general technique for following the movement of molecules inside cells, or cells inside embryos. It is particularly powerful for following the slowest exchanging component of a complex system. The potential advantages of, and requirements for, photoactivable fluorescent probes have been discussed elsewhere (Krafft et al., 1986), and the synthesis of probes that are photoactivated to fluorescein mono-ethers reported (Krafft et al., 1988). It is probably premature to compare C2CF with the probes developed by Krafft et al., but I note two points: (*a*) C2CF is activated to a fluorescein, rather than a fluorescein mono-ether. Fluorescein has a higher absorption coefficient, and a higher quantum efficiency of fluorescence emission

than its mono-ethers (Miller, 1983; Haugland, 1989). (*b*) The probes of Krafft et al. are likely to be more water soluble than C2CF in its present form. I hope to improve the water solubility of C2CF by introducing polar groups in the future.

Spindle Dynamics: Rapid Changes after Photoactivation

When activated zones were imaged a few seconds after activation they were bright and homogeneous. This image changed over the next 90 s or so to a dimmer, less homogeneous signal. I interpret the initial image as fluorescence from both marked kinetochore and marked astral microtubules. Most activated monomeric tubulin would have diffused away from the site of activation by 3 s (Salmon et al., 1984; Saxton et al., 1984). Nonkinetochore microtubules turn over with a half-life of less than a minute at 37°C, whereas kinetochore microtubules are much more stable (Mitchison et al., 1986). Thus I interpret the still localized signal remaining after 90 s as coming from marked zones restricted to kinetochore microtubules. Consistent with this explanation, the remaining fluorescence in PtK2 cells resolved into distinct bars parallel to the spindle axis with the distribution expected for individual marked kinetochore fibers. Electron microscopy would be required to confirm this identification. From the data in Figs. 7 and 8, I estimate that 25–50% of the initial label was retained after 90 s, which is reasonable for ratio of kinetochore to nonkinetochore microtubules measured by electron microscopy (Rieder, 1982).

Spindle Dynamics: Polewards Flux

In essentially all the cells that remained in metaphase long enough for observation, fluorescent zones on kinetochore microtubules moved slowly polewards. I interpret this observation as indicating that fixed points on the lattice of kinetochore microtubules move continuously polewards during metaphase; i.e., that there is polewards flux in kinetochore fibers. This polewards flux was obvious from movies (Figs. 6 and 7) and it was confirmed by two different digitizing approaches (Figs. 7 and 8). In PtK2 cells, where it was possible to image marked zones on individual kinetochore fibers, they seemed to flux polewards at similar, but nonidentical rates (Fig. 7). Polewards flux in kinetochore microtubules implies that they are polymerizing continuously at their plus ends attached to kinetochores (Euteneuer and McIntosh, 1981), and depolymerizing at their polewards minus ends. Polymerization of plus ends at kinetochores was first seen in vitro (Mitchison and Kirschner, 1985), and then in living cells by biotin-tubulin injection during metaphase (Mitchison et al., 1986). The segments of kinetochore microtubules that had incorporated injected subunits increased in length with time. This led to our predicting that continuous polewards flux occurs in kinetochore microtubules during metaphase. The observation of polewards movement of fluorescent marks in this study confirms the existence of such flux. The flux predicted from biotin-tubulin polymerization was strikingly similar to that observed directly in this study. In particular the flux rate was ~0.5 μm/min in both cases, and individual kinetochore fibers exhibited different flux rates. The qualitative and quantitative agreement between two methods with largely nonoverlapping methodological caveats represents the strongest evidence that such flux is an integral feature of the normal mitotic spindle.

Total localized fluorescence decreased with time during polewards movement (Fig. 10). I estimate that typically one-third of the marked subunits in kinetochore microtubules moved all the way to the poles. The remaining two-thirds became delocalized during the polewards movement process. This could be due to turnover of kinetochore microtubules, or to depolymerization of labeled subunits from the minus ends of kinetochore microtubules distributed throughout the fiber (Rieder, 1981). Assuming this loss was due to turnover only, it would imply a half-time for turnover of kinetochore microtubules of ~5 min. This is in reasonable agreement with an earlier estimate of about one microtubule per kinetochore per minute based on electron microscopy (Mitchison, 1988*b*), but both these estimates are very crude, and more quantitative work is required.

I have termed the dynamic behavior of kinetochore microtubules "polewards flux" rather than "treadmilling" for an important reason. Treadmilling was a term coined to describe balanced polymerization and depolymerization from opposite ends of a polymer driven by a difference in subunit affinities at the two ends (Margolis and Wilson, 1981). This difference in affinities derives from nucleotide triphosphate hydrolysis by the polymer (Wegner, 1976; Hill and Kirschner, 1982). Treadmilling is an important and specific class of nonequilibrium polymer behavior, and I prefer not to use its name to describe movement driven by as yet unknown factors. I cannot at present determine whether polewards flux in kinetochore fibers is driven by treadmilling or by other energy sources such as the action of translocating ATPases.

Comparison with Photobleaching Data

I am currently unable to explain why polewards movement of marked zones in tissue culture cell spindles was detected by photoactivation but not by previous photobleaching studies (Salmon et al., 1984; Saxton et al., 1984; Wadsworth and Salmon, 1986; Gorbsky and Borisy, 1989). The same cell lines were used, and the experimental conditions were broadly similar. Factors that may have lead to the detection of polewards microtubule flux in this study include the following. (*a*) The photoactivation method targets the observation to kinetochore microtubules, whereas photobleaching has a severe signal-to-noise problem following them in the spindle (see Introduction). However, I cannot explain why flux was missed in experiments in which bleached cells were permeabilized under conditions removing soluble subunits and most astral microtubules (Gorbsky and Borisy, 1989). (*b*) Photobleaching of fluorochromes could have led to photochemical cross-linking of microtubules to adjacent structures (Leslie et al., 1984) or to heat-induced local damage (Vigers et al., 1988). However, I would expect photodynamic damage by photobleaching to have led to perturbation of spindle function that was not observed. (*c*) The relatively low temperature (30–31°C) in this study increased the ratio of kinetochore to nonkinetochore microtubules (Salmon and Begg, 1980) and may also have decreased the turnover rate of kinetochore microtubules.

Microtubule Depolymerization during Metaphase

Kinetochore microtubules maintain a constant average length during metaphase, but in all animal spindles (including this study) they undergo continuous lengthening and shortening as the paired chromatids oscillate on the metaphase plate (Bajer, 1982). During this oscillatory steady state, kinetochore microtubules polymerize at the kinetochore (Mitchison et al., 1986) and in PtK2 cells at least, this polymerization occurs alternatively on the two sister kinetochores such that only one is polymerizing at any given time (Mitchison, 1988*a*,*b*). Polymerization at a given kinetochore must be balanced by an equal amount of depolymerization. During oscillations, chromosomes frequently moved several micrometers polewards at rates of up to 3 μm/min. Because fluorescent zones never moved polewards at such fast rates, the microtubule depolymerization accompanying these polewards movements cannot have occurred at the poles. By inference, microtubules must have depolymerized at kinetochores during metaphase chromosome oscillations, as they do in anaphase. This suggestion requires direct testing. It leads to a picture of the spindle where subunits exchange rapidly in and out of kinetochore microtubules at the metaphase plate, while the lattice moves more slowly polewards.

Implications of Polewards Flux for Spindle Structure

We already know that the connection between micotubule plus ends and kinetochores is a dynamic one (Mitchison, 1988*a*). The observation of polewards flux implies that the anchorage of kinetochore microtubule minus ends must also be dynamic, that is, that these ends can depolymerize while remaining attached to the spindle. The minus ends of many kinetochore microtubules in tissue culture cells are thought to be anchored in or near pericentriolar material at the poles, although some minus ends are distributed throughout the kinetochore fiber (Rieder, 1981). How are dynamic connections at the pole likely to work? Studies of microtubule nucleation by interphase centrosomes in vitro provided no evidence of dynamics at the minus ends anchored to the nucleating structure (Mitchison and Kirschner, 1984). The existence of polewards flux in living spindles demands that either microtubules nucleated by mitotic centrosomes do not have capped minus ends, or that kinetochore microtubules are not in fact nucleated from the centrosome, and are connected less directly to the pole. These interesting possibilities cannot yet be distinguished. It is clearly necessary to probe the structure and function of the mitotic pole in more detail, and to reexamine the idea that kinetochore microtubules are connected to the spindle by lateral interactions with polar microtubules (Bajer and Mole-Bajer, 1972; Nicklas, 1971; Nicklas et al., 1982).

Implications of Polewards Flux for Spindle Function

One puzzle of the flux observation is its relative slowness. The marked zones progress polewards at ~25% of the rate of anaphase chromosome to pole movement. This slowness makes it likely that the majority of anaphase depolymerization of kinetochore microtubules in tissue culture cells occurs at kinetochores as previously reported (Mitchison et al., 1986; Gorbsky et al., 1988). However, the existence of flux implies a potential redundancy in mechanisms for polewards chromosome movement. It is quite possible that microtubule depolymerization at the pole could account for more, or indeed all, of chromosome movement in other species. What role might slow polewards flux play in the spindles reported here? One possibility is a role in congression movements. The rate that chromosomes move from their initial site of attachment to the spindle to the equatorial plate is very variable, perhaps indicative of multiple mechanisms: some chromosomes (typically the first to congress) get to the equator by a series of large, fast saltatory jumps. Others (typically late arrivers) move much more slowly and steadily, taking 10 min or more to traverse the half spindle, and thus moving at a rate comparable to the flux rate. Another quite common form of congression occurs when a pole is slowly extruded away from the jiggling mass of chromosomes. This movement also takes about 10 min. Metaphase flux, slow congression movements, and polar extrusion all require kinetochore microtubules to move relative to cytoplasm at similar rates, with their minus ends leading. Thus all could manifest a common mechanism. An erstwhile popular model to explain the balancing of chromosomes on the metaphase plate postulated the existence of a polewards force acting per unit length of kinetochore microtubules (Ostergren, 1951; Hays et al., 1982). Kinesin-like ATPases pulling microtubules polewards relative to some spindle matrix are a plausible candidate for generating such a length dependent force (Vale, 1987). For such a force to achieve congression requires that congression movements are achieved at least in part by depolymerization at the polewards end of kinetochore fibers (discussed in Mitchison, 1988*b*). Thus, the observation of polewards flux in metaphase kinetochore fibers is consistent with the force per unit length model.

I am deeply indebted to Marc Kirschner for discussions during the theoretical development of this project and for providing space and resources, to David Trentham for my introduction to photoactivation chemistry and for encouragement, and to Jon Minden for invaluable help with chemistry and image processing. I also wish to thank Bob Schadel for making the epi-tube mirror, Gary Borisy and Victoria Centonze for providing LLC-PK1 cells; Vikus Bushan for help with image analysis; and Tony Hyman, Andrew Murray, and Vivian Siegel for valuable discussions.

This work was supported by the Medical Research Council, UK, National Institutes of Health grant GM-39565, the David and Lucile Packard Foundation, and the Lucille P. Markey Foundation through the University of California, San Francisco light microscopy facility.

Received for publication 17 February 1989 and in revised form 18 April 1989.

Note Added in Proof: The following improvements have been made in the synthesis of C2CF. After hydrolysis of intermediate 3, intermediate 4 is purified by chromatography on silica gel using benzene/methanol 1:1 as eluant. This additional chromatography step reduces the amount of fluorescent contaminants in the final preparation. The last synthetic step is now performed with a twofold molar excess of sodium *N*-hydroxysulfosuccinimide and dicyclohexylcarbodiimide over intermediate 4. After 24 h, the DMSO solution is filtered, extracted with ether as before, and excess sulfosuccinimide is precipitated with 2 vol of ethyl acetate, leaving the C2CF-sulfoNHS ester in solution. Compound 5 is then precipitated with 5 vol of benzene. This gives a more reproducible yield of activated ester.

References

Babcock, D. F., and D. C. Kramp. 1983. Spectral properties of fluorescein and carboxyfluorescein. *J. Biol. Chem.* 258:6389.

Bajer, A. S. 1967. Notes on the ultrastructure and some properties of transport within the living mitotic spindle. *J. Cell Biol.* 33:713–720.
Bajer, A. S. 1982. Functional autonomy of monopolar spindle and evidence of oscillatory movement in mitosis. *J. Cell Biol.* 93:33–48.
Bajer, A. S., and J. Mole-Bajer. 1972. Spindle dynamics and chromosome movements. *Int. Rev. Cytol.* 3(Suppl.): 1–264.
Bradford, M. M. 1976. A rapid and sensitive method for quantitation of microgram quantities of protein utilizing the principle of protein-dye binding. *Anal. Biochem.* 72:248–254.
Euteneur, U., and J. R. McIntosh. 1981. Structural polarity of kinetochore microtubules in PtK1 cells. *J. Cell Biol.* 89:338–345.
Forer, A. 1965. Local reduction of spindle fibre birefringence in living Nephrotoma suturalis (Loew) spermatocytes induced by ultraviolet microbeam irradiation. *J. Cell Biol.* 25:95–117.
Gorbsky, G. J., and G. G. Borisy. 1989. Microtubules of the kinetochore fiber turnover in metaphase but not in anaphase. *J. Cell Biol.* 109:653–662.
Gorbsky, G. J., P. J. Sammak, and G. G. Borisy. 1988. Microtubule dynamics and chromosome motion visualized in living anaphase cells. *J. Cell Biol.* 106:1185–1192.
Hamaguchi, Y., M. Toriyama, H. Sakai, and Y. Hiramoto. 1987. Redistribution of fluorescently labeled tubulin in the mitotic apparatus of sand dollar eggs and the effects of taxol. *Cell Struct. Funct.* 12:43–52.
Haugland, R. P. 1989. Molecular probes catalogue. Available from Molecular Probes, Eugene, OR.
Hayes, T. S., D. Wise, and E. D. Salmon. 1982. Traction force on a kinetochore fibre at metaphase acts as a linear function of kinetochore fibre length. *J. Cell Biol.* 93:374–382.
Hill, T. L., and M.-W. Kirschner. 1982. Bioenergetics and kinetics of microtubule and actin filament assembly-disassembly. *Int. Rev. Cytol.* 78:1–125.
Hiramoto, H., M. S. Hamaguchi, Y. Nakano, and Y. Shoji. 1984. Colcemid UV-microirradiation method for analyzing the role of microtubules in pronuclear migration and chromosome movement in sand-dollar eggs. *Zool. Sci. (Tokyo).* 1:29–34.
Inoue, S., and H. Sato. 1967. Cell motility by labile association of molecules. The nature of mitotic spindle fibres and their role in chromosome movement. *J. Gen. Physiol.* 50:259–292.
Jacobsen, K., A. Ishihara, and R. Inman. 1987. Lateral diffusion of proteins in membranes. *Annu. Rev. Biophys.* 49:1673–1675.
Kaplan, J.-H., B. Forbush, and J. F. Hoffman. 1978. Rapid photolytic release of adenosine 5'-triphosphate from a protected analogue: utilization by the Na:K pump of human red blood cell ghosts. *Biochemistry.* 17:1929–1935.
Kirschner, M. W., and T. J. Mitchison. 1986. Beyond self-assembly: from microtubules to morphogenesis. *Cell.* 45:329–342.
Kellogg, D. R., T. J. Mitchison, and B. M. Alberts. 1988. Behavior of microtubules and actin filaments in living *Drosophila* embryos. *Development (Camb.).* 103:675–686.
Krafft, G. A., R. T. Cummings, J. P. Dizig, L. J. Brvenik, W. R. Sutton, and B. R. Wars. 1986. Fluorescence activation and photodissipation (FDP). *In* Nucleocytoplasmic Transport. R. Peters and M. Trendelenberg, editors. Springer-Verlag, New York. 35–52.
Krafft, G. A., W. R. Sutton, and R. T. Cummings. 1988. Photoactivable fluorophores. 3. Synthesis and photoactivation of fluorogenic difunctionalized fluoresceins. *J. Am. Chem. Soc.* 110:301–303.
Leslie, R.-J., W.-M. Saxton, T.-J. Mitchison, B. Neighbors, E.-D. Salmon, and J.-R. McIntosh. 1984. Assembly properties of fluorescein-labeled tubulin in vitro before and after fluorescence bleaching. *J. Cell Biol.* 99: 2146–2156.
Margolis, R. L., and L. Wilson. 1981. Microtubule treadmills: possible molecular machinery. *Nature (Lond.).* 293:705–711.
McCray, J. A., L. Herbette, T. Kihara, and D. R. Trentham. 1980. A new approach to time resolved studies of ATP requiring biological systems: laser flash photolysis of caged ATP. *Proc. Natl. Acad. Sci. USA.* 77:7237–7241.
Miller, A.-G. 1983. Ethylated fluoresceins: assay of cytochrome P-450 activity and application to measurements in single cells by flow cytometry. *Anal. Biochem.* 133:46–57.
Mitchison, T. J. 1988*a*. Microtubule dynamics and kinetochore function in mitosis. *Annu. Rev. Cell Biol.* 4:527–549.
Mitchison, T. J. 1988*b*. Chromosome alignment at mitotic metaphase: Balanced forces or smart kinetochores? *In* Cell Movement. Vol 2. F. D. Warner and J. R. McIntosh, editors. Alan R. Liss, Inc., New York. 421–430.
Mitchison, T., and M. Kirschner. 1984. Microtubule assembly nucleated by isolated centrosomes. *Nature (Lond.).* 312:232–237.
Mitchison, T. J., and M. W. Kirschner. 1985. Properties of the kinetochore in vitro. II. Microtubule capture and ATP-dependent translocation. *J. Cell Biol.* 101:766–777.
Mitchison, T. J., L. Evans, E. Schulze, and M. Kirschner. 1986. Sites of microtubule assembly and disassembly in the mitotic spindle. *Cell.* 45: 515–527.
Nicklas, R. B. 1971. Mitosis. *Adv. Cell Biol.* 2:225–297.
Nicklas, R. B., D. F. Kubai, and T. S. Hays. 1982. Spindle microtubules and their mechanical associations after micromanipulations during anaphase. *J. Cell Biol.* 95:91–104.
Ostergren, G. 1951. The mechanism of coordination in bivalents and multivalents. The theory of orientation by pulling. *Hereditas.* 37:85–156.
Rieder, C. L. 1981. The structure of the cold stable kinetochore fibre in metaphase PtK1 cells. *Chromosoma (Berl.).* 84:145–158.
Rieder, C. L. 1982. The formation, structure, and composition of the mammalian kinetochore and kinetochore fiber. *Int. Rev. Cytol.* 79:1–58.
Roos, U. P. 1976. Light and electron microscopy of rat kangaroo cells in mitosis. III. Patterns of chromosome behavior during prometaphase. *Chromosoma (Berl.).* 54:363–385.
Salmon, E. D., and D. A. Begg. 1980. Functional implications of cold stable microtubules in kinetochore fibres of insect spermatocytes during anaphase. *J. Cell Biol.* 85:853–865.
Salmon, E. D., R. J. Leslie, W. M. Saxton, M. L. Karow, and J. R. McIntosh. 1984. Spindle microtubule dynamics in sea urchin embryos: Analysis using a fluorescein labeled tubulin and fluorescence redistribution after laser photobleaching. *J. Cell Biol.* 99:2165–2174.
Sammak, P. J., and G. G. Borisy. 1988. Detection of single fluorescent microtubules and methods for determining their dynamics in living cells. *Cell Motil. Cytoskeleton.* 10:1–9.
Saxton, W. M., D. L. Stemple, R. J. Leslie, E. D. Salmon, M. Zavortinik, and J. R. McIntosh. 1984. Tubulin dynamics in cultured mammalian cells. *J. Cell Biol.* 99:2175–2186.
Schaap, C. J., and A. Forer. 1984. Video digitizer analysis of birefringence along the length of single chromosomal spindle fibres. *J. Cell Sci.* 65:21–40.
Schulze, E., and M. Kirschner. 1988. New features of microtubule behavior observed in vivo. *Nature (Lond.).* 334:356–359.
Staros, J. V. 1982. N-hydroxysulfosuccinimide active esters: bis(*N*-hydroxysulfosuccinimide) esters of two dicarboxylic acids are hydrophilic, membrane-impermeant, protein cross-linkers. *Biochemistry.* 21:3950–3955.
Vale, R. D. 1987. Intracellular transport using microtubule-based motors. *Annu. Rev. Cell Biol.* 3:347–378.
Vigers, G. P., M. Coue, and J. R. McIntosh. 1988. Fluorescent microtubules break up under illumination. *J. Cell Biol.* 107:1011–1024.
Wadsworth, P., and E. D. Salmon. 1986. Analysis of the treadmilling model during metaphase of mitosis using fluorescence redistribution after photobleaching. *J. Cell Biol.* 102:1032–1038.
Walker, J. W., G. P. Reid, and D. R. Trentham. 1988. Synthesis and properties of caged nucleotides. *Methods Enzymol.* 172:288–301.
Wegner, A. 1976. Head to tail polymerization of actin. *J. Mol. Biol.* 108: 139–150.